Kinetics of Helix Unfolding: Molecular Dynamics Simulations with Milestoning[†]

Krzysztof Kuczera,[‡] **Gouri S. Jas,**[§] **and Ron Elber*,**[∥]

Departments of Chemistry and of Molecular Biosciences, The University of Kansas, 1251 Wescoe Hall Drive, Lawrence, Kansas 66045, Department of Chemistry Biochemistry and Institute of Biomedical Studies, Baylor University Science Building, Baylor University, 101 Bagby Avenue, Waco, Texas 76706, and Department of Chemistry and Biochemistry, ICES, C0200, The University of Texas at Austin, Austin, Texas 78712

The unfolding process of a helical heteropeptide is studied by computer simulation in explicit solvent. A combination of a functional optimization to determine the reaction coordinate and short time trajectories between "milestones" is used to study the kinetics of the unfolding. One hundred unfolding trajectories along three different unfolding pathways are computed between all nearby milestones, providing adequate statistics to compute the overall first passage time. The radius of gyration is smaller for intermediate configurations compared to the initial and final states, suggesting that the kinetics (but not the thermodynamics) is sensitive to pressure. The transitions are dominated by local bond rotations (the ψ dihedral angle) that are assisted by significant nonmonotonic fluctuations of nearby torsions. The most effective unfolding pathway is via the N-terminal.

Introduction

The phenomenon of peptide dynamics has been the subject of intensive studies from both experimental and theoretical perspectives. Computer simulations have the potential to provide a wide range of information about this process, yielding microscopic insight into the pathways and rates of conformational transitions, including the characterization of rarely sampled intermediates.[1,2] The progress in computational studies of peptide dynamics and folding may be divided into several stages, with progressive improvements in the methodology and investigations of larger systems. Early studies used direct molecular dynamics (MD) and free energy simulations of secondary structure elements,[1] followed by extensive simulations of helices, sheets, and miniproteins with first implicit and later explicit solvent models.[1,2]

Early studies included following unfolding of helices and turns, performed at elevated temperatures or with umbrella sampling.[1,3] These simulations found individual helical hydrogen bond breaking occurring at tens to hundreds of picoseconds and stabilities of sheets significantly greater than for helices. Pioneering work involved 2.2 ns length explicit solvent MD trajectories of YPDGV, a turn-forming pentapeptide, for which folding and unfolding were found on the nanosecond time scale,[4] and clustering was applied to analyze the conformational space and structural transitions.[5] Other studies employed the LES methodology for more comprehensive exploration of conformational space and determination of peptide structures CHDLFC[5] and SYPFDV,[6] illustrating significant correlation between the experimental structure and optimized peptide conformations.

More extensive calculations were initially performed using implicit solvation.[2] For the blocked (AAQAA)₃ peptide, microsecond simulations with a solvent model involving a distance-

dependent dielectric function and a solvent-accessible surface area term described the conformational free energy surface and folding as a function of temperature.[7] A single free energy minimum was found at all studied temperatures, corresponding to a folded state in the low-temperature range and an unfolded state at higher temperatures. Cluster analysis showed that folding proceeded through multiple nucleation events. Simulations by Duan and co-workers using the generalized Born (GB) implicit solvent model suggested that folding of alanine-rich helical peptides proceeded through several stages: three stages for the blocked YG(AAKAA)₂AAKA peptide[8] and two for the Fs-21 peptide, AAAAA(AAARA)₃A.[9] Important results for folding of helices, sheets, and small proteins were obtained using replica exchange MD (REMD).[2] These studies showed that explicit solvent REMD can correctly predict the global free energy minima for small model helix-forming[10] and hairpin-forming[11,12] peptides and others.[13] Good agreement between the calculated and observed melting temperature of Fs was obtained after adjustment of the AMBER force field.[10] The time scales for hairpin formation were estimated to fall in the microsecond range using energy landscape theory.[11] REMD with the GB/surface area (SA) implicit solvation gave incorrect results in some cases, predicting a helix−turn−helix structure for Fs and hydrophobic residues on the surface for the harpin-forming GB1 peptide.[2] In our joint experimental−computational study of the WH21 peptide,[14] we found generally good agreement between the GB/SA REMD simulations employing the CHARMM[15] force field and measured properties. The simulations found that the α helix was the system free energy minimum at low temperatures, and predicted an enthalpy change of −10 kcal/mol and an entropy change of −30 cal/(mol K) for the folding transition, quite similar to the experimental values of −11.6 kcal/mol and −39.6 cal/(mol K).[14]

Significant progress in enhancing the rate of conformational exploration was achieved with introduction of the REMD method.[2,16] REMD aims at thermodynamics and not at kinetics, which is the focus of the current investigation. Recent techniques to study kinetics include hyperdynamics,[17,18] transition path

sampling,[19] and sampling biased along an order parameter such as the TIS,[20] PPTIS,[21] forward flux,[22] and milestoning.[23]

Current computer power enables simulation of the folding equilibrium of peptides in aqueous solution using MD. Examples are a β-hexapeptide,[24] CW1 and CW2,[25] and Ala5.[26] With application of highly distributed computing systems, a significantly longer peptide, the 21-residue Fs system, has been studied.[27] The overall picture is that methods for equilibrium simulations are well developed, with accuracy limited by potential function development,[2,27] while a systematic computational description of peptide folding kinetics is only beginning to emerge.

In the present study we use the reaction path (RP) approach. RP studies of the kinetics and thermodynamics of peptide conformational transitions were initiated by Czerminsiki and Elber[28,29] and were (significantly) exploited further by Wales.[30] A variant of the peptide we investigate in the present study was studied by stochastic path optimization by Cardenas and Elber.[31] Comprehensive sampling of conformational space is simpler in the RP approach compared to MD simulations. However, significant questions remain. Lack of explicit solvent, inaccuracies of the models for effective solvation (especially for kinetics), and the use of energy minima (with implicit solvent) instead of free energy add to the uncertainties of these investigations.

Milestoning[23,32−35] aims to solve some of the RP problems by combining features of the RP and MD. Short time trajectories are computed in the neighborhood of the reaction coordinates, and a coarse-grained stochastic model for the motions is developed.[23] This strategy makes it possible to investigate the kinetics in much larger systems.[34] In the present study our efforts focus on early events in the unfolding of a helical peptide. Unfolding is more appropriate for a study with the reaction path approach than folding. This is because, close to the unfolded state, the number of alternative conformations is large and the reaction coordinates create a large network. The network of unfolded structures is dense and more difficult to describe with few reaction coordinates. The conformations closer to the folded state and states lower in free energy are likely to be sparse and accessible to this approach as suggested also from analysis of a very large number of trajectories.[27] Future studies will address the more comprehensive structure of the folding network.

Theory

Reaction Paths. The question of how to choose an RP to describe a complex condensed-phase problem is an important challenge that attracted and continues to attract timely research. There are two reasons for the significant interest in the RP. The first is qualitative understanding of the reaction progress, and the second is quantitative comparison to experimental data.

Atomically detailed simulations retain the coordinates of all atoms as a function of a parameter (typically time), monitor the progress of the reaction, and allow for comprehensive data mining of the reaction dynamics. However, the comprehensive picture is not something we can easily understand and use. Typically we describe and quantify the process using a model of reduced complexity. We discuss bond breaking in aqueous solutions and not the motion of individual water molecules surrounding the reaction center. We describe complex conformational transition in peptides and proteins by a sequence of events that include local bond rotations, hydrogen bond formations, and shifts of secondary structure elements (see for instance ref 36). The sequence of events can be tested experimentally by probing the time evolution of different degrees of freedom.[37]

We do not consider in detail the Cartesian displacements of protein atoms.

The qualitative information extracted from the RP provides a simple, easy to understand picture of the process. However, to study function, we need to connect the structural and energetic information with kinetic and thermodynamic properties. This second task of linking structure to function can also be addressed by the RP. A widely used approximate approach is the transition-state theory (TST). If the energy barrier separating the reactants and product is significantly larger than kT, a rate constant can be computed with different variants of this theory and corrections to it.[38]

If our interest focuses on qualitative insight of reaction mechanisms, then many options are possible that vary from theoretically derived most-probable Brownian trajectories,[39] or trajectories that maximize the flux,[40] to heuristic such as targeted molecular dynamics[41] or an assumed internal coordinate. However, our focus in the present paper is two-fold.

The first goal is indeed to study mechanisms. However, we also aim to obtain a quantitative estimate of the rate of folding (or unfolding) along particular reaction coordinates. The RP of choice in the present study is the steepest descent path. In many calculations of reaction coordinates one ignores the kinetic energy of the system and determines the RP according to the properties of the potential energy surface. For example, the steepest descent path (SDP) is widely used in chemistry and is a continuous curve with a low-energy barrier that connects the reactants and the products. At any point along the SDP we find at most one negative eigenvalue of the second-derivative matrix of the potential energy. An important advantage of an SDP is that it allows the test of a concrete mechanism. The disadvantage of the SDP approach lies in the multiplicity of possible paths. The three paths considered in the present study examined unfolding mechanisms that are initiated differently.

Given the above classification, we realize that there are two types of reaction coordinates to simulate folding. The first type (widely used in the past in studies of folding) is of a collective variable selected by intuition, for example, the end-to-end distance of a polymer or the number of native contacts. The second type, which is used in the present study, is the SDP widely used in studies of small molecules. These two classes reflect different philosophies of the RP.

The collective variable usually corresponds to a single-order parameter that monitors the progress of the reaction. Indeed the number of native contacts is a useful probe for the folding/unfolding state of the system and was used extensively in theoretical and computational studies of protein folding.[42] Nevertheless, there are two difficulties in the use of collective variables as reaction coordinates in computational studies of kinetics.

The first is sampling in the orthogonal space to the reaction coordinate. For the unfolded state (zero native contacts) the number of conformations is extremely large, which makes computational exploration of this state (for a fixed number of native contacts) very difficult. It also makes the calculation of kinetics problematic, since one usually assumes a separation of time scales between times for motion along the reaction coordinate and times for motion in the direction perpendicular to it. For the vast space orthogonal to the reaction coordinate such separation is hard to justify.

The second difficulty is qualitative interpretation of the results. Typical collective variables tend to average multiple mechanisms and mask interesting dynamics at the molecular level. For

Kinetics of Helix Unfolding

J. Phys. Chem. A, Vol. 113, No. 26, 2009 **7463**

example, the end-to-end distance cannot capture the importance of a specific bond rotation.

When an SDP is used as a reaction coordinate, we have a different scope in mind. The SDP is constructed numerically as a set of images along a line. The line has a minimum energy barrier separating the reactants and products. We have no information on the properties of the system far from the curve connecting the set of images. We therefore approximate the space orthonormal to the reaction coordinate by a hyperplane and assume that trajectories do not deviate significantly from the SDP line. It is easier to justify time scale separation within this picture since the space orthogonal to the reaction coordinate is typically small and can be explored quickly. Mechanisms are also easier to identify within the SDP picture. The challenge is that a single SDP cannot provide a comprehensive view of the process. Other SDPs may have significant contributions, and pipes may cross and split, creating a complex network of transitions. Furthermore, the relative weights of different SDPs need an extra calculation, a task left for future work.

We generate the SDPs of the present study from initial guesses. The initial paths were selected from equilibrium replica exchange simulations in implicit solvent. The details of these studies were reported elsewhere.[14] Replica exchange calculations in conjunction with implicit solvent models explore alternative conformations rapidly and offer a rich bank of alternate structures to choose from to build initial guesses for the folding pathways.

Once an initial guess for the reaction coordinate is available, we optimize the path in two steps. In the first step the self-penalty walk (SPW) algorithm is used.[43] The SPW algorithm is a robust and fast algorithm that provides reasonable approximations to the SDP. The output path from the SPW algorithm is used as a starting point for an optimization of another functional that rigorously provides the steepest descent path:[39]

$$F[q(l)] = \int_{\mathbf{X}_R}^{\mathbf{X}_P} \sqrt{\nabla U^t \nabla U} \, \mathrm{d}l \qquad (1)$$

The reaction coordinate is q, the gradient of the potential energy is ∇U, $\mathbf{X}_R$ and $\mathbf{X}_P$ are the coordinate vectors of the reactants and the products, respectively, and $\mathrm{d}l$ is a length element along the reaction coordinate $\mathrm{d}l = (\mathrm{d}\mathbf{X}^t \cdot \mathrm{d}\mathbf{X})^{1/2}$. It was shown in ref 39 that a minimum of $F(q(l))$ is indeed the SDP. We also called the algorithm of eq 1 "optimization of a scalar force" to indicate that we optimize the norm of the potential gradient (and not the potential gradient itself). A discrete representation of the functional was introduced, making it possible to compute numerically the SDP.

The above functional form is particularly convenient to study complex systems. One of the reasons is that the end points are fixed, ensuring a "successful" transition from reactant to product. This is an outcome that is hard to get in initial value calculations of reaction coordinates. In that sense eq 1 is similar to other boundary value formulations of the SDP such as the LUP algorithm[44] and numerically enhanced implementations of LUP (the NEB[45] and the zero temperature string[46]). The approach in eq 1 is different from those of the above three since it is formulated as a minimization of a functional. Having a target function at hand enhances stability and allows in principle larger steps. It also makes it possible to use stochastic optimization techniques (such as Monte Carlo) for the SDP without explicit calculations of the derivatives of the functional. Nevertheless, the algorithm in eq 1 is in general slower than approaches that rely on potential derivatives. In our case, since the calculations of the reaction path are only a negligible component of the
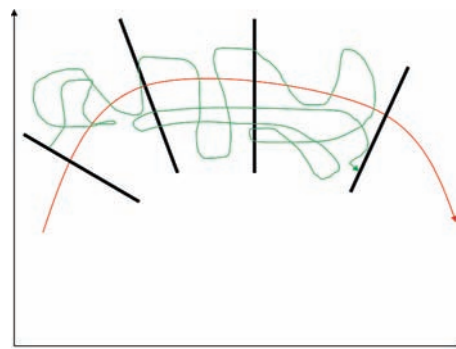

Figure 1. A schematic view of milestoning. The red arrow is the reaction coordinate, and in green we draw an exact reactive trajectory that is initiated at the reactants (R) and is terminated at the last interface (P). The interfaces are shown as thick black lines orthonormal to the reaction coordinate.

computational cost, we have used directly eq 1 as implemented in the molecular dynamics modeling package MOIL (module sdp).[47] The output of the calculation is three SDP paths that are used in the milestoning calculations.

Milestoning. Milestoning is an approximate simulation technique to study kinetics at long time scales while retaining the atomically detailed description of the system.[33,34] It is based on the availability of milestones, interfaces along the reaction pathway connecting the reactants and products (Figure 1). Consider an exact trajectory that is initiated at the reactants and ends at the products. It may pass many times back and forth through the milestones, but it "hits" the product state only once. The product state is absorbing, and the trajectory is terminated after the first touch of the final milestone.

An ensemble of trajectories of this type provides the reaction rate as a function of time. For example, the number of molecules in the reactant state $N_R(t)$ at time t is frequently modeled by an exponential decay as a function of time:

$$N_R(t) = N_0 \exp[-\lambda t] \qquad (2)$$

The number of trajectories initiated in the reactant state is N_0, and λ is the apparent rate constant. The difficulty in estimating rate constants by straightforward simulations of individual trajectories and fitting the data against eq 2 is the cost. Because of limited computer power molecular dynamics trajectories are typically restricted to the submicrosecond time scale. An ensemble of such trajectories would be (of course) significantly more costly. Milestoning makes it possible to compute the ensemble of reactive trajectories at a fraction of the cost, which in the present example is at least 1000.

In milestoning we assume that an equivalent representation of reactive trajectories can be assembled from short trajectories between milestones (Figure 2). Trajectories are renewed at the interfaces by sampling from a predetermined stationary distribution at the interface. In the present study we restrict our attention to conditions close to thermal (canonical) equilibrium. However, any known stationary distribution can be used, even far from equilibrium, as long as it represents a steady flux. The renewal is done with a fixed value of the reaction coordinate in the hypersurface orthonormal to the reaction coordinate at i and not necessarily at the point in which the trajectory we wish to renew was terminated. This loss of memory in the interface differentiates milestoning from other transition path sampling procedures (such as TPS,[19] TIS,[20] and forward flux,[22] which continue the terminated trajectory from the same point at which it was stopped). The spatial memory loss of milestoning can be made exact with a special choice of the reaction coordinate and
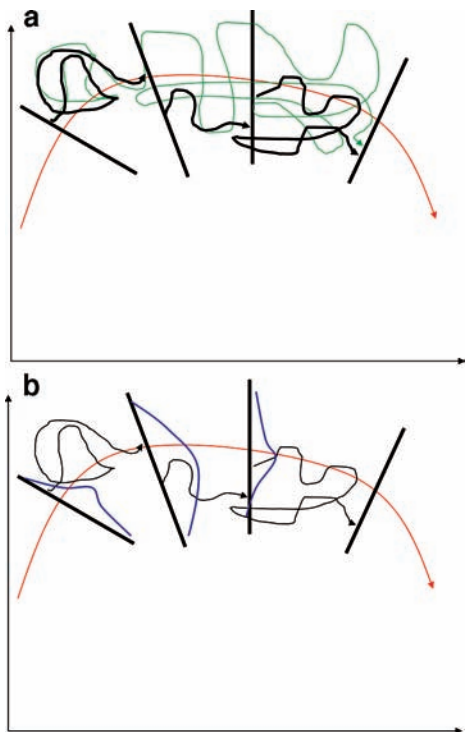
Figure 2. A schematic picture of the milestoning approximation. A complete exact trajectory is shown in green as in Figure 1. Also shown are fragments of a trajectory in black (a). There are three trajectory fragments that we "glue". The assumption is that the relaxation times in the hyperplane perpendicular to the reaction coordinate are short. Therefore, we can sample from equilibrium at the interface, and the short relaxation times at the interface (compared to the transition time between the milestones) can be ignored. Since we have an ensemble of trajectories, it should not matter (provided that our assumption is correct) where we initiate the trajectory at the interface. Also shown in blue lines (b) are the probability densities of terminating trajectories at the milestones. If we know the probability densities of the terminating trajectories, we can sample the fragmented trajectories directly from these distributions. In previous[23,33,34] and current applications of milestoning, we assume that equilibrium densities can approximate the terminating distributions. A distribution that provides an exact first passage time is found in ref 35, and a new intriguing numerical protocol to sample these distributions was proposed in ref 48.

the dynamics.[35] However, in general it is an approximation. The approximate resampling at the interface overcomes a significant statistical problem (getting a statistically meaningful number of trajectories to terminate at a particular interface). It allows us to push the time scales that we can study with molecular dynamics significantly further than is possible with other algorithms. It also allows us to investigate processes that do not follow exponential kinetics and mix diffusion and hopping over barriers. Below we consider in more detail the approximations made in milestoning, and then we discuss why the calculations are significantly more efficient.

There are two ways of thinking about the above approximation (Figure 2).

The first considers a single trajectory. If the time of relaxation to equilibrium within the hyperplane perpendicular to the reaction coordinate is much shorter than the transition time between the milestones, then the relaxation time within the plane can be ignored. The total reaction time is just the sum of transition times between the milestones. This view suggests a clear way to test the milestoning approximation and to improve it. Since we are working with a finite number of interfaces, increasing the distance between the interfaces will better satisfy the separation of the time scale

(the time scale for the relaxation within the interface remains the same, while the time scale for the transition between the interfaces increases as we increase the separation). However, the computational efficiency of milestoning decreases with a decrease in the number of interfaces. Therefore, a compromise between accuracy and efficiency should be made.

The second view, which is subtler and discussed extensively in ref 35, is based on the time evolution of the probability density. Instead of the motion of one trajectory at a time, we consider the time evolution of an ensemble of trajectories. Let the probability density of trajectories that terminate in the hyperplane perpendicular to milestone i be $\rho_i(\Gamma)$, where Γ denotes the orthogonal hypersurface. This probability density is our best (exact) choice for renewing the trajectories at i. Unfortunately, this probability density is not known exactly except in special cases.[35] The probability density is therefore approximated by an analytical function or using a simulation. An analytical approximation we have used in the past is that of an equilibrium distribution.[33,34] Of course the terminating trajectories generate samples of the exact distributions at the nearby interfaces, and the approximate form of the density can be tested for consistency. A computational technique that directly generates these distributions, and is still significantly more efficient than straightforward molecular dynamics, was proposed recently[48] and is a very promising direction.

We define the mean first passage time (MFPT) $\langle t \rangle$ as the time averaged over an ensemble of trajectories that are initiated at the reactants (milestone 1) and terminated at the products (milestone N). The last milestone (products) is absorbing. The MFPT captures characteristics of the time evolution of the process. For example, if the reactant population, $N_R(t)$, decays exponentially as a function of time, $N_R(t) = N_0 \exp(-\lambda t)$, then the rate constant λ is given by $1/\langle t \rangle$. To compute the overall MFPT, we use the formula developed in ref 32, which was illustrated in ref 33 and rederived in ref 35. For completeness of this paper we define the relevant variables, explain how they are extracted from the simulation, and provide the final formula.

We define $K_{ij}(\tau)$ as the probability density that a trajectory initiated at milestone i at time $\tau' = 0$ will transition to milestone j at time $\tau' = \tau$. The time integral $\int_0^\infty K_{ij}(\tau)\, d\tau = p_{ij}$ is the transition probability from state i to state j. The sum over all final states is normalized, $\sum_j p_{ij} = 1$. The last (products) milestone is absorbing, and $p_{NN} = 1$. We also define the transition matrix:

$$[\mathbf{K}(\tau)]_{ij} = \begin{Bmatrix} K_{ij}(\tau) & i \neq j \\ 0 & \text{otherwise} \end{Bmatrix} \tag{3}$$

The mean first passage time is then given by

$$\langle t \rangle = \mathbf{1}^t \cdot \int_0^\infty \tau \mathbf{K}(\tau)\, d\tau \cdot [\mathbf{I} - \int_0^\infty \mathbf{K}(\tau)\, d\tau]^{-1} \cdot \mathbf{Q}_i \tag{4}$$

The symbols $\mathbf{1}^t$, $\mathbf{I}$, and $\mathbf{Q}_i$ are a vector of all ones $(1, 1,..., 1)$, the identity matrix, and a projection vector onto the initial milestone $(1, 0,..., 0)^t$, respectively. From eq 3 it is obvious that the transition matrix $\mathbf{K}$ plays a dominant role in determining the kinetics of the system. Indeed in our previous papers on milestoning and in the present study we estimate this matrix numerically by sampling. We initiate trajectories at each milestone i according to a Boltzmann distribution, constrained to the hypersurface at i, $\rho_i(\Gamma)$:

$$\rho_i(\Gamma)\, d\Gamma = Z^{-1} \delta(q - q_i) \exp[-\beta U(X)]\, d\Gamma$$
$$Z = \int dX \exp[-\beta U(X)] \tag{5}$$

We denote the reaction coordinate by q, the complete coordinate space by X, and the space complementary to q by Γ. We record

Kinetics of Helix Unfolding

J. Phys. Chem. A, Vol. 113, No. 26, 2009 **7465**

the termination times of the trajectories at milestone j. The number of termination events from milestone i to milestone j, $L(i{\to}j;\tau,\tau+\Delta\tau)$, is counted during the time interval $[\tau,\tau+\Delta\tau]$. We divide $L(i{\to}j;\tau,\tau+\Delta\tau)$ by the total number of trajectories initiated at i, L_i, to estimate $K_{ij}(\tau)\Delta\tau$ with the proper normalization:

$$K_{ij}(\tau)\Delta\tau \cong \frac{L(i{\to}j;\tau,\tau+\Delta\tau)}{L_i} \qquad (6)$$

Since all trajectories initiated at i terminate in the limit of long time we also have

$$L_i \equiv \sum_{j,k=1,\ldots,\infty} L(i{\to}j;k\Delta\tau)\Delta\tau$$

Estimating the elements of the transition matrix and their time dependence is necessary if the complete time evolution of the system is of interest (e.g., compute $N_R(t)$ for a general, not necessarily exponential, process). The theory and some examples of these general processes are discussed in detail in ref 33. The essence is a numerical solution of an integral equation for the probability of being at milestone i at time t. These general calculations can be expensive since they require significant sampling of the three-dimensional tensor $K_{ij}(\tau)$ (including the time "dimension").

On the other hand, eq 4, which provides the overall mean first passage time, includes only integrals of the probability density, $K_{ij}(\tau)$, that are easier to estimate and require significantly less statistics. We have estimated the MFPT in the study of the allosteric transition of scapharca hemoglobin[34] using a relatively small number of trajectories. We focus on the MFPT also in the present study of folding/unfolding of a helical peptide.

So far we have discussed the theory and the implementation of milestoning. However, we have not discussed why milestoning is beneficial compared to straightforward molecular dynamics. In ref 33 it was argued that the computational gain of using milestoning compared to straightforward molecular dynamics is proportional to the number of milestones if the process is diffusive and is exponential in the number of milestones for activated transitions (states separated by a significant free energy barrier). For the completeness of this paper we repeat the qualitative arguments below. We also illustrate (as part of this paper) that the milestoning calculations of helix folding are more efficient than straightforward molecular dynamics by a factor of thousands, enabling meaningful calculation of rates in complex systems.

Consider first a diffusive process along a (one-dimensional) reaction coordinate. If the diffusion is on a "flat" energy surface (we shall consider the other limit next), then the time t it diffuses along a path length Y would be proportional to Y^2 (from the relationship $Dt{\sim}Y^2$, where D is the diffusion constant). In milestoning we consider diffusion between the M interfaces. Each pair is roughly separated by a $Y/(M-1) \approx Y/M$ distance. The time of transition between two interfaces is therefore proportional to $(Y/M)^2$. The total time of a transition between M interfaces is $M(Y/M)^2 = Y^2/M$.

The computational time to observe a transition in milestoning is therefore a factor of M shorter than a straightforward trajectory. We typically use close to 100 milestones, so the computational gain is substantial. Consider next a significant barrier separating the two minima. If the system is close to thermal equilibrium, then the probability of making it to the top of the barrier is proportional to $\exp[-\beta\Delta U]$, where β is the inverse temperature and ΔU the barrier height with respect to the reactants. However, if we divide the reaction path from the

reactants to the top of the barrier by M milestones, then the probability of reaching the next milestone is about $\exp[-\beta\Delta U/M]$. Since we initiate the trajectories at a milestone, the computational cost of computing the corresponding ensembles is proportional to a sum (instead of the product we have in MD):

$$\text{cost(milestoning)} \propto \sum_{i=1,\ldots,M} \exp[\beta\Delta U/M]$$

$$\text{cost(MD)} \propto \exp[\beta\Delta U] = \prod_{i=1,\ldots,M} \exp[\beta\Delta U/M] \qquad (7)$$

For a typical number of milestones (about 100), the gain can be staggering.

Computational Protocol

Selection of Initial Seeds for the Reaction Coordinates. The use of a sample of SDP pathways that we propose in the present paper allows us to test concrete mechanisms, test their consistency with experimental data, and learn about the characteristics of the transition. The guiding trajectories for helix unfolding pathways were generated using previous REMD simulations of the blocked WH21 peptide[14] (sequence WA$_3$HA$_3$RA$_4$RA$_4$RA$_2$). Both the N-terminal and C-terminal are uncharged. The N-terminal is capped with a COCH$_3$ group, while the C-terminal is terminated with an NH$_2$ group. The simulations used eight replicas with temperatures spanning 280−450 K, a GB/SA continuum solvation model, and the CHARMM program.[15] In a 30 ns long REMD trajectory starting from an α-helical structure, conformational equilibrium was reached after 15 ns. For the unfolding transition this simulation predicted a melting temperature T_m of 330−350 K, an unfolding enthalpy $\Delta H = -10$ kcal/mol, and an entropy $\Delta S = -30$ cal/(mol K). These values were in reasonable agreement with the experimentally observed values of $T_m = 296$ K, $\Delta H = -12$ kcal/mol, and $\Delta S = -40$ cal/(mol K).[14] Our second REMD simulation was 15 ns in length and started from the extended structure. In this case, the helical conformation was first attained after ca. 2.8 ns and equilibrium was reached after 10 ns.

We generated three helix−coil transition paths from the structures sampled in the GB/SA REMD simulations. For path 1 we employed the sample of 37 500 structures from the 367 K replica in the 30 ns ("equilibrium") simulation, classified by the root-mean-square deviations (rmsd's) of backbone atoms from an ideal helix and the number of α-helical hydrogen bonds (NAHB) for each structure. The subset with NAHB = 8 was hierarchically clustered on the basis of the backbone rmsd using the MMTSB tool set.[49] The path was initiated by selecting a random structure from the largest cluster, and a series of intermediates was then identified by analysis of pairwise rmsd and NAHB, producing a chain of 16 structures spanning the range of NAHB = 17 (corresponding to the α-helix) to NAHB = 0 (fully unfolded state). For the second path, we selected three structures from the 298 K replica of the 30 ns equilibrium REMD−one corresponding to the α-helix (NAHB = 17), the second to the unfolded C-terminal portion of WH21 (with NAHB = 8 and hydrogen bonds formed in the N-terminus only), and the third to the coil state (NAHB = 0). The third path was constructed from the first 2.8 ns of the 298 K replica of the 15 ns ("folding") simulation in which the helix is formed from an extended conformation. In this case we again used rmsd and NAHB analysis to find 15 structures spanning from NAHB = 17 to NAHB = 0.

In our analysis we did not count the hydrogen bonds of the blocking groups. The backbone rmsd between the nearest neighbors in the chains varied from 0.7 to 2.5 A. The paths

selected were arbitrary, in the sense that they do not correspond to any directly simulated transitions, but represent roughly random walks through configuration space constrained to follow a roughly sequential, or zipper, hydrogen bond breaking/ formation mechanism with limited rmsd changes between neighbors. We chose the generation methods to make the paths as different as possible. Thus, for path 1 the initial structures were sampled from above the simulated T_m, where the population of partially unfolded intermediates is higher than at 298 K, and the path was required to pass through the most highly populated NAHB = 8 intermediate. Path 2 was based on the same REMD simulation, but only three structures from the 298 K replica were employed in the initiation, and the intermediate was arbitrarily selected to correspond to the unfolded C-terminal of WH21. Finally, path 3 was initiated on the basis of the structures sampled in the 298 K replica of the folding simulation, using that part of the trajectory in which the system first converts from coil to helix in the course of the random walk generated by the combined MD and MC that are part of the REMD algorithm.

In the next stage of path generation, the initial chains underwent iterative interpolation and optimization using the SDP algorithm, producing paths with 77 milestones for path 1, 129 milestones for path 2, and 113 milestones for path 3. These paths are complete in the sense that they start at the folded (helix) state and end at the unstructured (zero hydrogen bonds) conformation. The number of alternative paths grows very rapidly as a function of the distance from the folded state. Therefore, time scales calculated along one-dimensional paths are likely to be overestimated, since transition to the unfolded state is made to any of many unstructured conformations. Therefore, most of the detailed analysis presented in the Results and Discussion is done on the path in the neighborhood of the helix. There the number of alternative paths is smaller and time scale estimates are more likely to be meaningful.

Path Calculations. Optimization of the initial guesses for intermediate structures along the paths follows. To speed up convergence, the minimum energy paths were computed in two steps. The structures along the guess path were fed first to the SPW algorithm[43] (module chmin in MOIL[47] and https://wiki.ices.utexas.edu/clsb/wiki). The optimized paths are computed with the discrete representation of a line integral with equidistance restraints introduced by Elber and Karplus[50] and further refined by Czerminski and Elber.[51] This type of restraint was adopted by the NEB[45] and by the Maxflux[40] algorithms for calculations of reaction coordinates. In brief, the line integral is approximated by a finite difference expression:

$$S[X(l)] = \int_{X_R}^{X_L} G(X(l)) \, dl \cong \sum_{i=1}^{N-1} G(X(l_i))\Delta l_{i,i+1} +$$
$$\sum_i \lambda(\Delta l_{i,i+1} - \langle \Delta l_{i,i+1} \rangle)^2 + \sum_i \rho \exp\left[-\frac{\kappa \Delta l_{i,i+2}^2}{\langle \Delta l_{i,i+2} \rangle^2}\right] + EC \tag{8}$$

In the context of the present paper the integrand $G(X(l))$ can be either $U(X)/L$ in the SPW algorithm[51] (L is the path length) or $(\nabla U^t \nabla U)^{1/2}$ in the calculations of the SDP.[39] The discrete length element is given by $\Delta l_{i,i+1} = [(X_{i+1,s} - X_{i,s})^t(X_{i+1,s} - X_{i,s})]^{1/2}$. The path constraints apply to only a subset of the coordinates that are the Cartesian positions of the C_α atoms of the peptide. This subset is denoted by the index "s" in the above formula for the distance $\Delta l_{i,i+1}$. The parameter λ restrains all length elements to be similar to the average $\langle \Delta l_{i,i+1} \rangle$, and the term with

the next nearest neighbor distance ($\Delta l_{i,i+2}$) reduces the path curvature. The restraint on the next nearest neighbor distance was not used in the SDP calculations. The last term (EC) is the Eckart conditions expressed as six linear constraints[33] (three on translation and three on overall rotations). The path is optimized with a conjugate gradient minimizer or simulated annealing subject to the above linear constraints as a function of all the intermediate structures X_i.

Structures along the path were added between intermediate conformations to ensure that the difference between sequential structures did not exceed 0.6 Å rms after optimal overlap and optimization of the functional. The results of the SPW optimization were input to compute three different SDP paths with a discrete form of the functional of eq 8.[39] The optimizations are assumed converged when no significant changes in the structures are observed with more optimization cycles.

The paths are computed using the package MOIL with the generalized Born model for solvation,[52] but are otherwise in a vacuum. Water molecules are not included in the calculation of the SDP since the flat energy surface for solvent molecules and their permutations suggest low-energy barriers and high degeneracy for their motions. The floppy solvent structure at room temperature does not support the use of a minimum energy path model, and the generalized Born model mimics a potential of mean force more appropriate in the present context. Explicit solvation is (of course) included in the calculations of the short-time milestoning trajectories.

Milestoning Calculations. To compute short terminating trajectories between milestones, we follow two steps: (i) sample configurations in the milestones to generate an initial stationary distribution at the interfaces and (ii) integrate trajectories initiated from the sample of step I and Maxwell velocity distribution until the trajectories terminate on nearby milestones. Once a set of terminating trajectories and their corresponding time lengths are recorded, we use eq 4 to estimate the overall first passage time of the early events of the folding/unfolding transition of the peptide.

In preparation for step i, we solvate the peptide in a cubic box of water of 41.8³ Å³ with periodic boundary conditions for each peptide configuration, $q(l_i)$, along the SDP. The water model is TIP3P[53] (the geometry of the water molecules is fixed with the matrix-SHAKE algorithm[54,55]). The force field is united atom OPLS[56] as implemented in our code MOIL.[47] Four chloride ions were added to ensure electric neutrality, and particle meshed Ewald[57] was used to sum electrostatic interactions. The Lennard-Jones interactions were truncated at 8 Å, and the time step was 0.5 fs. We first equilibrate the solvent for 20 ps around the frozen configurations of the peptide (from the SDP calculations). The system is coupled to a heat bath by velocity scaling in the first 20 ps (velocity scaling or the isokinetic ensemble ensures canonical ensemble of configurations[58]). The remaining 20 ps was run in the NVE ensemble. The system is sufficiently large so that the differences between an assigned temperature and computed temperature from the average kinetic energy are small. The standard deviations of the temperatures in the NVE ensembles along the paths are less than 10 K′. The last coordinate sets of the trajectories of solvent (plus frozen peptide) are saved and used as starting points for simulations to generate the stationary distributions at the interface

The NVE simulations in the hyperplanes orthogonal to the reaction coordinate are ordinary molecular dynamics simulations of the peptide and solvent supplemented by linear constraints.[33] The simulation parameters are the same as in the previous simulations equilibrating the solvent except that now the peptide

Kinetics of Helix Unfolding

J. Phys. Chem. A, Vol. 113, No. 26, 2009 **7467**

is allowed to move. The MD trajectories remain in the designed milestone through application of the constraint

$$(\mathbf{X}_s - \mathbf{q}_{si}) \cdot \mathbf{e}_{si} = 0 \qquad \mathbf{e}_{si} \cong \frac{\mathbf{q}_{si+1} - \mathbf{q}_{si-1}}{|\mathbf{q}_{si+1} - \mathbf{q}_{si-1}|} \qquad (9)$$

The constraint is enforced with Lagrange's multiplier (appendix of ref 33). The coordinate vector of the system is $\mathbf{X}$, and its projection onto the subset of the selected variables (the Cartesian positions of the C_α atoms) is $\mathbf{X}_s$. The unit vector $\mathbf{e}_{si}$ is normal to hyperplane i along the reaction coordinate. The normal (which is $\mathbf{e}_{si}$) and a point in the hyperplane (which is $\mathbf{q}_{si}$) determine the position of the interface uniquely. Since the constraint is expressed in Cartesian coordinates, it is also necessary to fix the global orientation and position of the molecule. This is achieved by six (linear) constraints (derived from the Eckart conditions) in addition to the path constraints above. This is similar to the discrete path calculations discussed in eq 8 and discussed in detail in ref 33. The simulations were run in the NVE ensemble for 50 ps for each location along the reaction coordinate, and structures were saved every 0.5 ps. For each $\mathbf{q}_{si}$, we therefore have a sample of 100 conformations that are used to initiate the terminating trajectories between the milestones.

In the second phase, we compute molecular dynamics trajectories without the hyperplane constraint (eq 9) while retaining the six constraints on overall molecular orientations. We keep the six constraints to enable convenient determination of termination times. Trajectories that are initiated at $\mathbf{q}_{si}$ are stopped, and their times are recorded when $(\mathbf{X}_s - \mathbf{q}_{si-1}) \cdot \mathbf{e}_{si-1} = 0$ (termination at the previous milestone) or when $(\mathbf{X}_s - \mathbf{q}_{si+1}) \cdot \mathbf{e}_{si+1} = 0$ (termination at the next milestone). Since the vectors $\mathbf{q}_{sj}$ and $\mathbf{e}_{sj}$ are expressed in Cartesian coordinates which are sensitive to overall molecular motions, it is useful to constrain the C_α to a fixed overall orientation. The constraints used in phase ii are softer than the constraints used in the sampling phase, and therefore, a larger time step (1 fs) is used without significant loss of accuracy. The rest of the simulation parameters are kept the same.

Typically trajectories are terminated after a few or tens of picoseconds. However, in extreme cases tens of nanoseconds are observed as well. Nevertheless, the trajectory times are much shorter than the computationally estimated time scale for folding or unfolding, which is in the microseconds (along one-dimensional paths), illustrating that milestoning is indeed a lot more efficient than straightforward molecular dynamics. For example, the accumulated time of all trajectories of the milestoning calculation of the first SDP is 68 ns. The computed first passage time for the transition was 2 μs, significantly longer than the time that was required to compute it.

The actual number of milestones that are finally used in the estimate of the overall mean first passage time may be smaller than the number of structures generated along the SDP. To improve the milestoning approximation, we make sure that the trajectories are not too short and memory loss between initiation of the trajectory and its termination is indeed achieved.[33] In practice, we found that the loss of velocity correlation is usually sufficient to obtain accurate results for the mean first passage time. We further determine empirically that for aqueous peptide systems 400 fs is usually enough to decorrelate the velocity along the direction parallel to the reaction coordinate. Therefore, if we sample termination times shorter than 400 fs between sequential milestones, we increase the separation between the milestones by taking one out. For example, rather than computing termination between milestones i and $i + 1$, we compute them between i, and $i + 2$. This extra calculation is not

TABLE 1: Number of Trajectories Initiated at a Milestone and Terminating at (a) the Milestone Forward and (b) the Milestone Backward[a]

	no. of trajectories forward/total
Path 1	
milestone before transition	44/100
milestone after transition	74/100
Path 2	
milestone before transition	116/133
milestone after transition	21/100
Path 3	
milestone before transition	34/100
milestone after transition	61/100

[a] The information was used to decide when the first barrier for unfolding was passed.

expensive since the trajectories below 400 fs are cheap to compute and add only little to the overall cost.

Results and Discussion

We consider the dynamics of helix unfolding along three reaction coordinates. In the first path (path 1) we consider unfolding initiated at the N-terminal. In the second path (path 2) the unfolding is initiated at the C-terminal, and in the third (path 3) the helix breaks in the middle, creating two short helices in the first step. Snapshots along the paths are shown in Figure 3. We consider in the text below the initiation of unfolding and the complete unfolding pathways.

When does the first step of unfolding end? We have used quantitative and qualitative measures to define the end of the beginning. First, we consider the reverse of the reactive flux in the milestoning calculations. We seek milestone i, which is closest to the first milestone of the helical conformation such that the direction of the net flux of trajectories is reversed. Let n_+ be the number of trajectories that are terminating in the forward direction and n_- the number of trajectories terminated in the backward direction. We seek a pair of milestone i and $i + 1$ such that $(n_+^i - n_-^i)(n_+^{i+1} - n_-^{i+1}) < 0$. Near a stable conformation the flux of trajectories points to that state. A change in the direction of the net flux suggests a transition over the top of a free energy extremum. The net flux is estimated by the number of trajectories that terminate in the next milestone minus the number of trajectories that terminate in the previous milestone. In Table 1 we list the number of trajectories between milestones that led to our decision in paths 1−3. Second, we verify this choice by visual inspection, requiring significant structural changes in the subset of coordinates at $q(l_i)$, where l_i is the index of the transition point. In retrospect the verification was not necessary since the flux condition works well. The "initiation" step of helix unfolding spans milestones 1−14 in the first path, milestones 1−58 in path 2, and milestones 1−13 in the third path. In the analysis below we focus on path 1, which provides a time scale consistent with experiment. The more significant barriers (and longer time scales) of paths 2 and 3 cannot be explained by a single dominant interaction, and the excess energy (and free energy) is spread over many degrees of freedom.

Calculations of Rate. The calculations of the complete unfolding rate along the three paths probe different processes compared to experiment. The calculations consider a transition from the helix into the neighborhood of only one unfolded conformation for each of the paths. The experiment considers a transition from the helix into any of the unfolded structures.
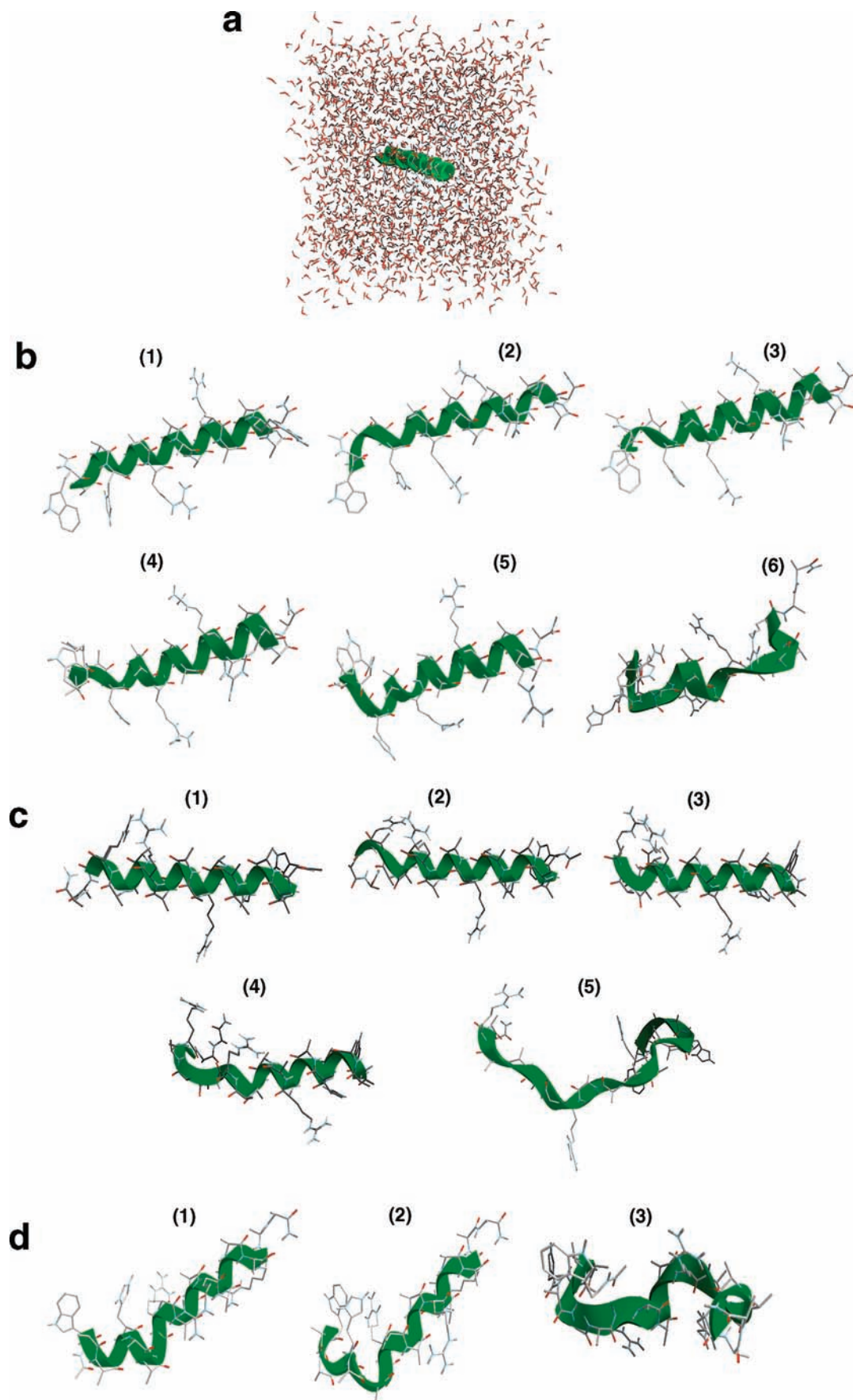
Figure 3. Structural snapshots along the three pathways. The images displayed in the present paper were prepared with the cmoil/zmoil program and the graphic display module of MOIL.[47] (a) Solvated structure of the helical conformation. For clarity the solvent was removed from all the structures that follow. Note also that in path 1 (b) the N-terminal is on the left while in path 2 (c) the C-terminal is on the left. Sequence of peptide structures along the (a) first path, (c) second path, and (d) third path.

Kinetics of Helix Unfolding

J. Phys. Chem. A, Vol. 113, No. 26, 2009 **7469**

TABLE 2: Time Scale for Transitions from Helical Conformations to the First Step in Unfolding and to the Unfolded Conformations[a]

	mean first passage time	
	unfolding time	elementary step
path 1	280 ns	455 ps
path 2	7 μs	1.58 ns
path 3	86 μs	8.9 ns

[a] The times are given for the three paths that we considered.

The larger number of choices of alternative final conformations in the experiment makes it likely that the computation will provide a lower bound to the rate. We expect that simulated rates will be similar to experimental data if the final structure chosen in the calculations is one of highly preferred unfolded shapes, and that computed rates will be slower if multiple pathways to other unfolded structures contribute similarly to the rate. Indeed the mean first passage times that we obtain for one-dimensional unfolding (Table 2) cover a diverse range of time scales, with the lowest values being comparable to the experimental rate. The relaxation rate is measured experimentally to be 3.3×10^6 s^{-1} at 300 K.[14,59] Nevertheless, these estimates are still within typical errors that are seen with other studies. Errors in the force field can easily change the rates by a factor of 10. Consider an activated process that follows an Arrhenius expression for the rate constant. Increasing the barrier height by 1.5 kcal/mol at 300 K, which is a typical error in condensed-phase simulations, reduces the rate constant by a factor of 12. It is therefore unclear whether the errors are a result of the assumed one-dimensional reaction coordinate, the force field, the milestoning approximation, or other factors. The initiation of unfolding events that we examined and their corresponding rates provide some support to the force field we used. These rates are not in significant variance with those observed in straightforward multiple MD trajectories,[27] suggesting that the results of our calculations are typical. We therefore continue to examine the mechanisms of unfolding along the paths.

The kinetics of the first steps of unfolding (starting from the helix) are more likely to describe accurately the experimental behavior when compared to the RP approach. Near the helix conformation the number of unfolding paths is small, and parallel independent paths is a reasonable description of the process. In the discussion below, we therefore focus on the early event; however, we also analyze properties of the complete folding pathway as appropriate.

Efficiency of the Calculations. In Figure 4a we show an example of a simulated first passage time distribution $K_{ij}(\tau)$ of transitions to two nearby milestones. To differentiate between trajectories that terminate in the forward and the backward directions, we use negative times to denote termination backward (on the previous milestone). It is obvious that the time scale of termination at the nearby milestones is significantly shorter than the time scale of the overall process (picoseconds versus microseconds). This illustrates the high efficiency of milestoning. Even with 48 milestones for the first path and 100 trajectories launched from each milestone (with a trajectory time of about 50 ps, which is on the high side), the accumulated time to compute the rate is $100 \times 48 \times 50$ ps = 240 ns, still significantly shorter that the time to compute a single trajectory probing the event. Note that for the calculations of the overall first passage time we need only the zero and the first moments of the above distribution. Therefore, despite the sparse sampling,
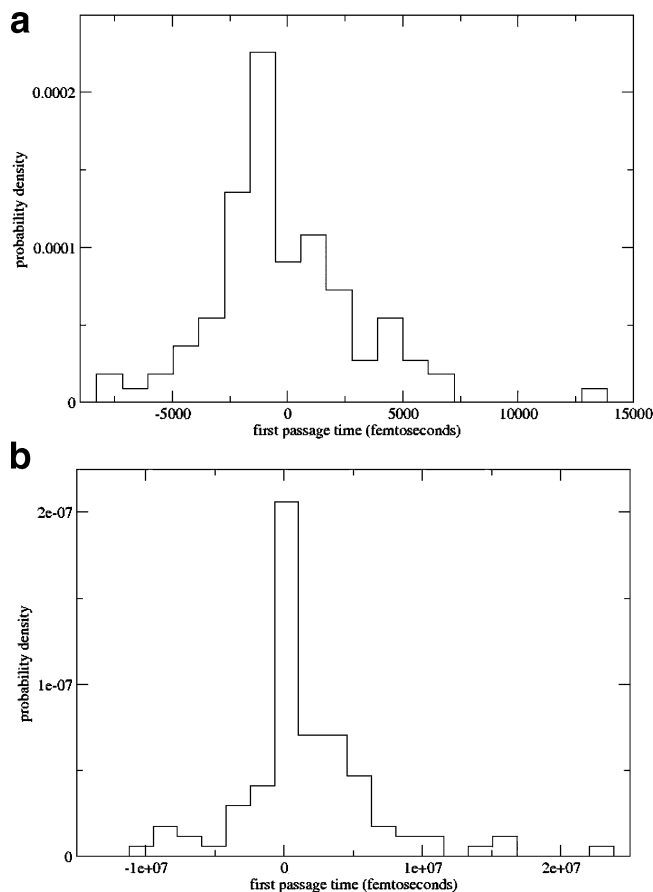

Figure 4. Local (between milestones) first passage time distributions. (a) Distribution sampled from milestone 15 of the first path. Negative times denote termination of the trajectories on the previous milestone and positive times termination in the forward direction. (b) Distribution computed from the third path.

we are able to obtain results with acceptable (but significant) statistical error bars. For example, halving the number of data points for the third unfolding path changes the time scale from 86 to 205 μs for the first 50 trajectories and to 79 μs for the last 50 trajectories. If our estimates are accurate enough, the time scales also suggest that the first path is significantly more likely from the kinetics viewpoint, even if thermodynamically configurations from all paths are observed in the replica exchange simulations.

An extreme distribution of $K_{ij}(\tau)$ from path 3 is shown in Figure 4b. The trajectories are considerably longer since a smaller number of milestones (29) was used along a less direct unfolding pathway compared to path 1. However an estimate similar to the one we did above suggests that milestoning is still more efficient than straightforward MD. The maximum termination time is 22 ns. A complete trajectory along all 29 milestones assuming the maximum time of transition for terminations at the milestones (which is clearly an upper bound) requires 638 ns. This is still shorter by about a factor of 100 compared to the overall first passage time (86 μs) we estimated for this path (Table 2).

Analyses of Structural Features of the Transition. The analysis of the path includes changes in local variables such as specific torsion angles and global variables that capture the shape of the peptide, e.g., the radius of gyration. Besides the representation of distributions of relevant spatial variables, there is significant interest in their time dependence. In our analysis we wish to capture both the spatial distributions of variables at
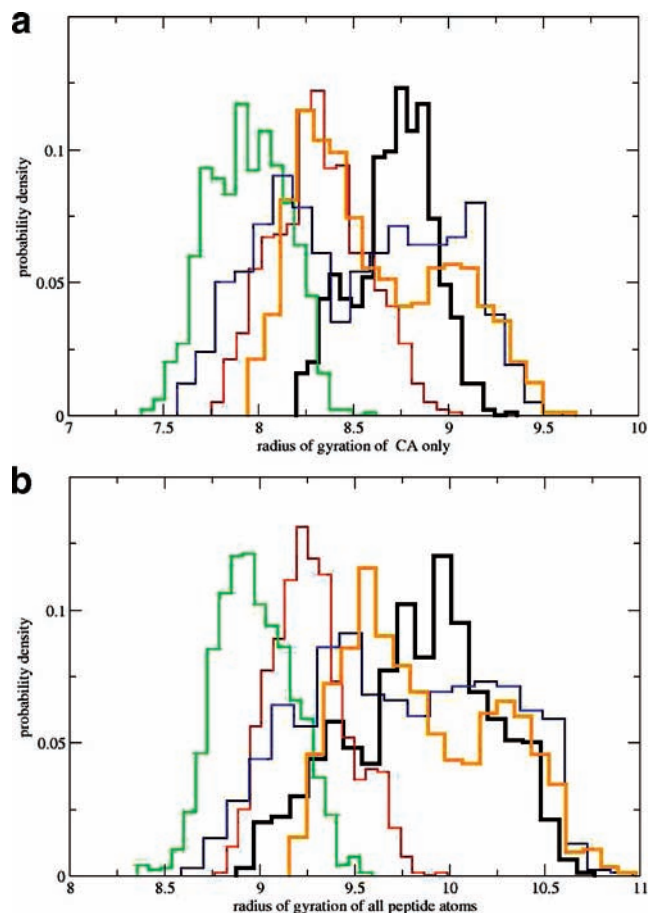
Figure 5. Probability density of the radius of gyration as a function of progress along the reaction coordinate for the first path. (a) Only C_α atoms are included in the calculation of the radius of gyration. (b) All atoms are included. The black histogram is the distribution for the helical conformation. Red, green, blue, and orange histograms follow sequentially the black curve along the path.

a given instance of time and their time evolution. In each of the following figures we show several graphs that are color coded to indicate their position along the reaction coordinate. The black curve corresponds to the initial helical phase, and the later time distributions are (in sequential order) red, green, blue, and orange.

Radius of Gyration. The complete path 1 is divided into five more-or-less equal segments. For example, the initiation of unfolding in the first path includes 18 milestones. The data presented in the graphs are collected from the conformational statistics generated from milestones 1, 5, 10, 15, and 18. In Figure 5a we show the variation in the radius of gyration of C_α for several milestones along the complete unfolding path (the C_α Cartesian coordinates define the space in which the reaction coordinate is optimized). The radius of gyration varies in value from about 7.5 Å for the most compact conformations to 9.7 Å for the most extended structures. These are not very large deviations, but they are nevertheless significant. The broadest distribution of radii of gyration is one step before complete unfolding (the blue curve), which is perhaps surprising. As we emphasized, however, the RP approach does not measure correctly the diversity of structures of the unfolded state. This is because the sampling is performed in the neighborhood of particular structural images. The width of the last distribution in orange is therefore wider than the folded state but is not wider than the intermediate (blue) distribution.

Another interesting observation is the nonmonotonic behavior of the radius of gyration. The sequence of black, red, and green histograms clearly shows the average radius of gyration shrinking. Hence, the backbone of the peptide (no side chains are considered) becomes more compact as unfolding is in progress. The red and green distributions are also not significantly broader than the distribution of the radii of gyration of the helix (first milestone sampling). Only the blue and the orange distributions that lean toward the unfolded state show significant broadening compared to the initial helical state. In contrast to the red and green distributions, they show an increase in the average value of the radius of gyration.

This observation also suggests that the use of the radius of gyration as an order parameter to probe unfolding is problematic. The nonmonotonic dependence of the radius of gyration on the RP makes it difficult to assign a position along the reaction coordinate given a value for the radius of gyration. The use of the radius of gyration as a reaction coordinate is therefore ambiguous. If we consider all the peptide atoms in Figure 5b (and not only C_α), the evolution of the pathway shares properties similar to those of the backbone-only path. Not surprisingly, the values of the radius of gyration are somewhat larger (the side chain atoms are now taken into account). However, we still observe the same qualitative trends of the compression of intermediate structures, and an increase in the average radius of gyration at late phases of the reaction (the blue and orange distributions). As before, the blue and orange distributions are also considerably broader.

The analysis of the radius of gyration along the RP puts forward an interesting experimental suggestion. Since the radii of gyration (or the overall volume) of the folded and unfolded states are similar (black and orange distributions), we do not expect a significant change in the equilibrium constant relating the two states as a function of pressure. On the other hand, the intermediate structures seem to have a smaller volume. Therefore, the theoretical prediction is that pressure will reduce the time scale of the transition but will keep (more or less) the equilibrium constant of the folded and unfolded states intact.

Another widely used measure of size is the end-to-end distance computed from the nitrogen of the N-terminal to the carbon of the carboxyl terminal. We show five histogram plots of the end-to-end distance distributions for path 1 in Figure 6. There is a clear and abrupt transition from a narrow distribution of distances at the helix conformation to a broad distribution of distances that consistently drift to more compact structures. The broad distributions overlap significantly, making it difficult to pinpoint a specific position along the reaction progress using the end-to-end distance. Interestingly, the picture of the end-to-end distance is significantly different from what we have seen from the radius of gyration. A similar view is obtained also for the initiation of unfolding.

The radius of gyration is a useful indicator of the compactness of the structure. However, other measures of shape can be useful. Honeycutt and Thirumalai[60] introduced two new shape measures constructed from the eigenvalues λ_i of the tensor of inertia (in addition to the radius of gyration). These measures were found useful in a number of studies of complex macromolecules.[61] The first is denoted by Δ and is defined by

Kinetics of Helix Unfolding

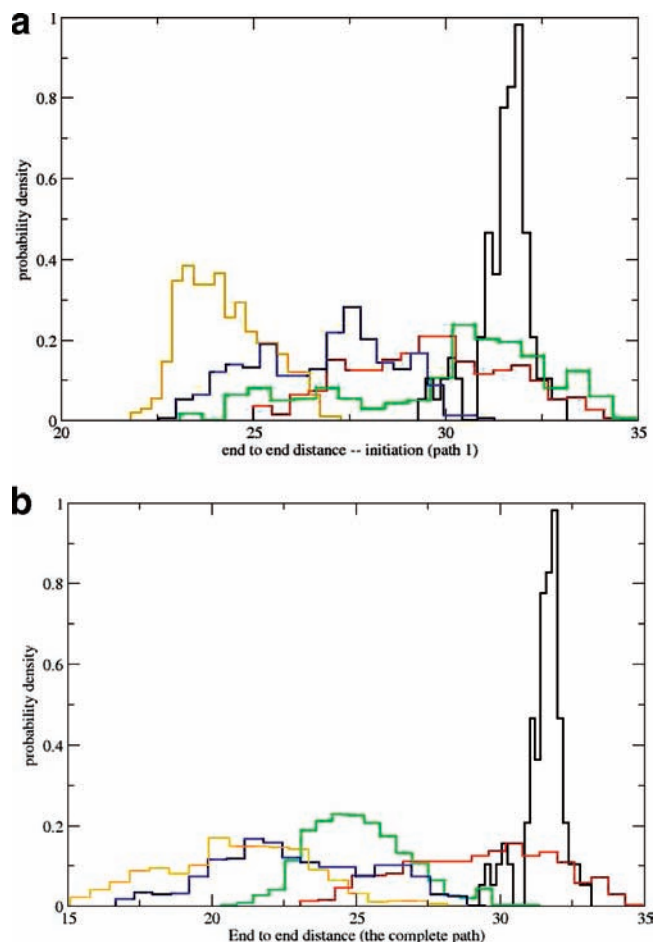*J. Phys. Chem. A, Vol. 113, No. 26, 2009* **7471**

Figure 6. Probability density of the end-to-end distance as a function of the reaction coordinate: (a) initiation of the unfolding pathway (up to milestone 18), (b) complete unfolding pathway of the first path. The histograms and colors are the same as in Figure 5.

$$\Delta = \frac{3}{2} \frac{\sum\limits_{i=1,2,3} (\lambda_i - \lambda^-)^2}{\left(\sum\limits_{i=1,2,3} \lambda_i \right)^2} \tag{10}$$

The eigenvectors of the tensor of inertia are λ_i. The average over the three eigenvalues is $\bar{\lambda}$. If the object is a sphere, all the eigenvalues are the same and Δ is zero, which is also its minimum. In Figure 7 we show that the unfolding transition starts at reasonably high values of Δ and sequential distributions are shifted to lower values. The lower values indicate shapes that are more spherical than the initial (and also the final) state. Indeed the significant deviations from a spherical shape of the initial helix milestone (the black histogram) and of the final unfolded milestone (orange bins) are similar in size and distribution. For the initiation of the first path (Figure 7b) we observe monotonic drift to more spherical shapes.

Another shape measure introduced by Honeycutt and Thirumalai is S:

$$S = 27 \frac{\prod\limits_{i=1,2,3} (\lambda_i - \lambda^-)}{\left(\sum \lambda_i \right)^3} \tag{11}$$

In contrast to the Δ parameter, S can be negative, for example, if one (and only one) of the eigenvalues is significantly smaller than the other two (and from the average). A "pita bread" shape
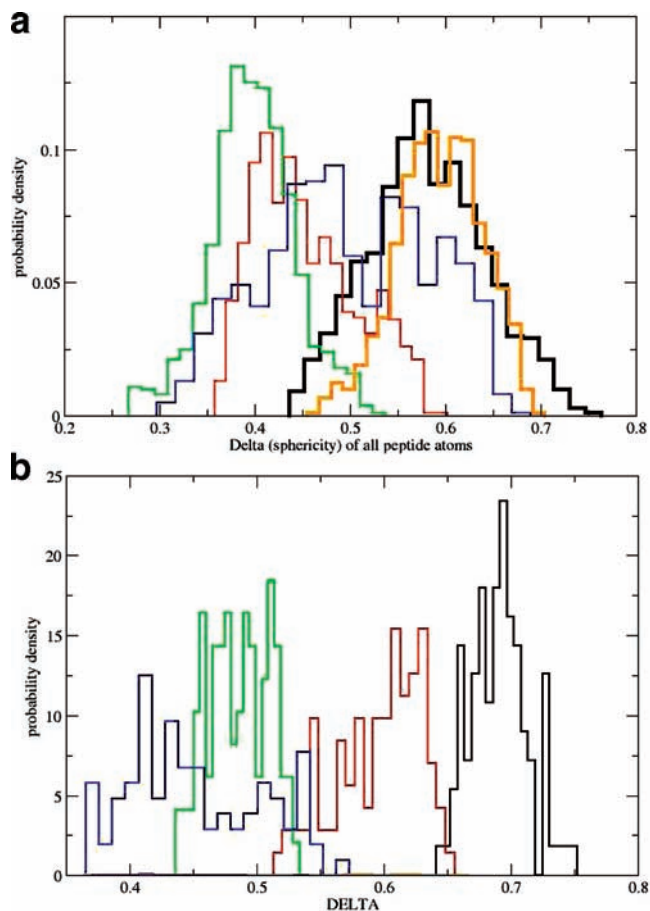

Figure 7. Probability density of the shape measure Δ for the first path: (a) complete path, (b) path initiation (up to milestone 18; also only four distributions are used for clarity, no orange). The histograms and colors are the same as in Figure 5.
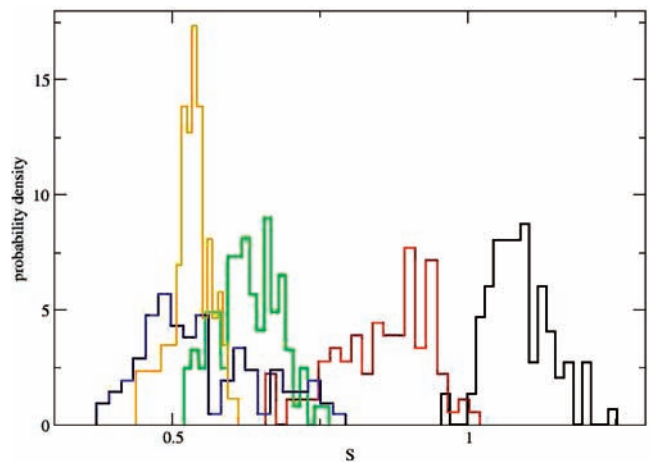

Figure 8. Probability density of the shape measure S for the initiation of the first path. The histograms and the colors are the same as in Figure 5.

will have a negative S. It is therefore of interest that our analysis never found negative S values, suggesting a transition from cigar shapes to closely spherical conformations. In Figure 8 we show that the changes (given only for the path initiation phase) clearly separate the states along the beginning of the unfolding pathway. The swollen configurations of the unfolded state were similar to those of the folded state using the measures of the radius of gyration and Δ. However, the last measure and the end-to end distance put the unfolded state in roughly the same domain as
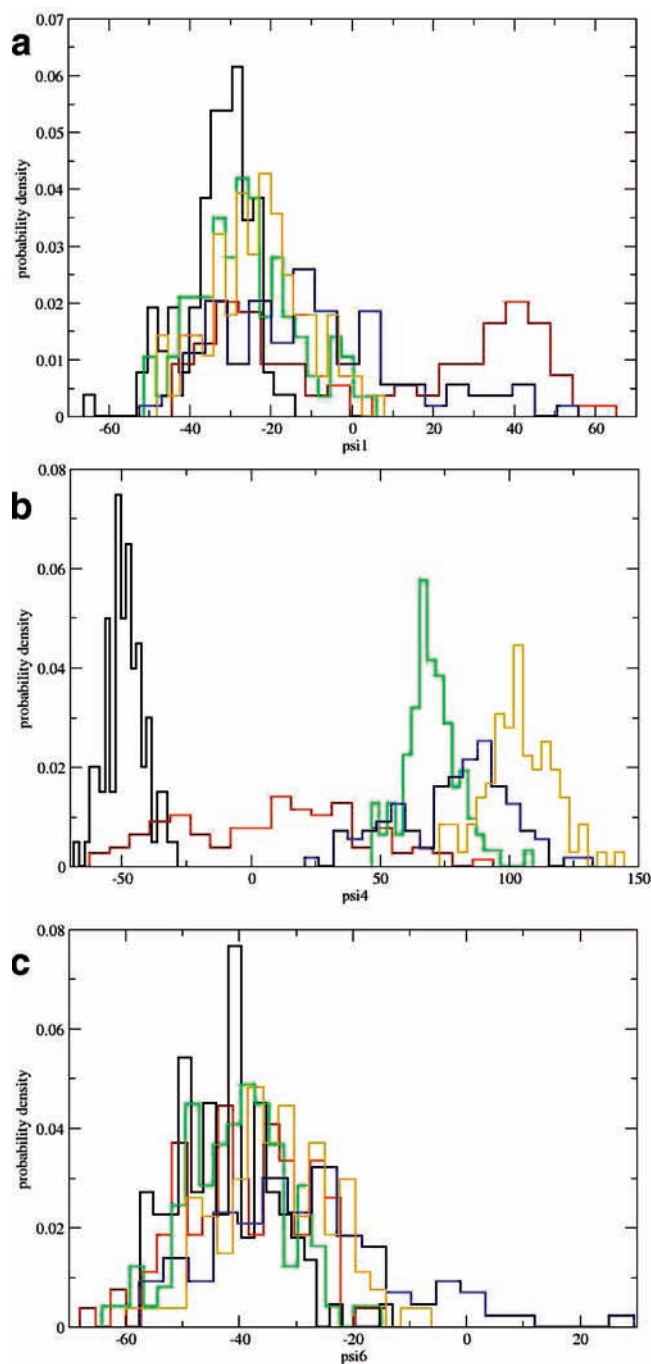
Figure 9. Probability densities for dihedral angle transitions along the first path: (a) ψ_1, (b) ψ_4, (c) ψ_6. The histograms and colors are the same as in Figure 5.

the intermediates.

It is also intriguing to examine local torsions. Peptide conformations are usually determined by the value of the ψ dihedral angles. The variations in ω are negligible, and the fluctuations in φ values are typically smaller than those of ψ. Even with the reduction in the number of relevant torsions, there are still 21 ψ torsions in the peptide under consideration, and we examined all of them. Detailing fluctuations of all 21 torsions in this paper can be exhausting and is not necessary. This is because these transitions tend to be local and we focus on the initial events of unfolding and the few active torsions. In Figure 9a we show the evolution of the distribution for the first torsion of interest ψ_1. The plot is surprising since the final distribution of the dihedral angle is concentrated near negative values of a

helical conformation. Of course, also the starting distribution is helical, making the unfolding process strongly nonmonotonic (going from a helix to an extended chain and back to a helix from the perspective of the first torsion). Only intermediate distributions (blue and red) "leak" to the extended chain but still maintain their hold in the helical configurations. The dihedral angle that does most of the work for initiation of the unfolding process is ψ_4. In Figure 9b we show a clear drift from a narrow distribution in the neighborhood of the helix to a diffusive (red) distribution that covers most of the accessible torsion space to different narrow distributions localized at the extended β sheet configurations. Torsion angles of residue 6 and higher are unaffected by the unfolding of the edge of the helix (Figure 9c). Similar localized transitions of dihedral angles assisted by large fluctuations of nearby torsions were found in other cases.

Concluding Remarks

We have illustrated how the combination of reaction paths and milestoning allows us to study in atomic detail the unfolding of a helical peptide. We are able to compute experimentally verifiable kinetics at a long time scale that will be instrumental in calibrating and assessing force fields. An interesting observation that our analysis found is that the intermediate structures are more compact compared to the initial (folded) and the final (unfolded) states. This qualitative prediction of more compact transitional states suggests that the kinetics can be made faster if the pressure in the system increases. Increasing the pressure will not affect significantly the equilibrium between the folded and unfolded configurations. Three paths are considered, N-terminal, C-terminal, and unfolding from the middle. The significantly shorter time scale of the first path and the proximity of the time scale to the experimental unfolding rate suggest that the N-terminal path is highly significant in accord with stochastic path calculations.[31] It will be of considerable interest to extend this study to a network of structural images representing milestones between folded and unfolded configurations with time courses of transitions determined by first passage time distributions.

References and Notes

(1) Brooks, C. L. *Acc. Chem. Res.* **2002**, *35*, 447.

(2) Gnanakaran, S.; Nymeyer, H.; Portman, J.; Sanbonmatsu, K. Y.; Garcia, A. E. *Curr. Opin. Struct. Biol.* **2003**, *13*, 168.

(3) Brooks, C. L. *Curr. Opin. Struct. Biol.* **1993**, *3*, 92.

(4) Tobias, D. J.; Mertz, J. E.; Brooks, C. L. *Biochemistry* **1991**, *30*, 6054.

(5) Karpen, M. E.; Tobias, D. J.; Brooks, C. L. *Biochemistry* **1993**, *32*, 412.

(6) Mohanty, D.; Elber, R.; Thirumalai, D.; Beglov, D.; Roux, B. *J. Mol. Biol.* **1997**, *272*, 423.

(7) Ferrara, P.; Apostolakis, J.; Caflisch, A. *J. Phys. Chem. B* **2000**, *104*, 5000.

(8) Chowdhury, S.; Zhang, W.; Wu, C.; Xiong, G. M.; Duan, Y. *Biopolymers* **2003**, *68*, 63.

(9) Zhang, W.; Lei, H. X.; Chowdhury, S.; Duan, Y. *J. Phys. Chem. B* **2004**, *108*, 7479.

(10) Garcia, A. E.; Sanbonmatsu, K. Y. *Proc. Natl. Acad. Sci. U.S.A.* **2002**, *99*, 2782.

(11) Garcia, A. E.; Sanbonmatsu, K. Y. *Proteins: Struct., Funct., Genet.* **2001**, *42*, 345.

(12) Zhou, R. H.; Berne, B. J.; Germain, R. *Proc. Natl. Acad. Sci. U.S.A.* **2001**, *98*, 14931.

Kinetics of Helix Unfolding

J. Phys. Chem. A, Vol. 113, No. 26, 2009 **7473**

(13) Simmerling, C.; Strockbine, B.; Roitberg, A. E. *J. Am. Chem. Soc.* **2002**, *124*, 11258.

(14) Jas, G. S.; Kuczera, K. *Biophys. J.* **2004**, *87*, 3786.

(15) Brooks, B. R.; Bruccoleri, R. E.; Olafson, B. D.; States, D. J.; Swaminathan, S.; Karplus, M. *J. Comput. Chem.* **1983**, *4*, 187.

(16) Sugita, Y.; Okamoto, Y. *Chem. Phys. Lett.* **1999**, *314*, 141.

(17) Voter, A. F. *Phys. Rev. Lett.* **1997**, *78*, 3908.

(18) Hamelberg, D.; Mongan, J.; McCammon, J. A. *J. Chem. Phys.* **2004**, *120*, 11919.

(19) Dellago, C.; Bolhuis, P. G.; Geissler, P. L. Transition path sampling. *Advances in Chemical Physics*; John Wiley & Sons Inc.: New York, 2002; Vol. 123; p 1.

(20) van Erp, T. S.; Bolhuis, P. G. *J. Comput. Phys.* **2005**, *205*, 157.

(21) Moroni, D.; Bolhuis, P. G.; van Erp, T. S. *J. Chem. Phys.* **2004**, *120*, 4055.

(22) Allen, R. J.; Frenkel, D.; ten Wolde, P. R. *J. Chem. Phys.* **2006**, *124*, 17.

(23) Faradjian, A. K.; Elber, R. *J. Chem. Phys.* **2004**, *120*, 10880.

(24) Daura, X.; Gademann, K.; Schafer, H.; Jaun, B.; Seebach, D.; van Gunsteren, W. F. *J. Am. Chem. Soc.* **2001**, *123*, 2393.

(25) Yeh, I. C.; Hummer, G. *J. Am. Chem. Soc.* **2002**, *124*, 6563.

(26) Buchete, N. V.; Hummer, G. *J. Phys. Chem. B* **2008**, *112*, 6057.

(27) Sorin, E. J.; Pande, V. S. *Biophys. J.* **2005**, *88*, 2472.

(28) Czerminski, R.; Elber, R. *J. Chem. Phys.* **1990**, *92*, 5580.

(29) Czerminski, R.; Elber, R. *Proc. Natl. Acad. Sci. U.S.A.* **1989**, *86*, 6963.

(30) Wales, D. J. *Energy Landscapes with Applications to Clusters, Biomolecules and Glasses*; Cambridge University Press: Cambridge, U.K., 2003.

(31) Cardenas, A. E.; Elber, R. *Biophys. J.* **2003**, *85*, 2919.

(32) Shalloway, D.; Faradjian, A. K. *J. Chem. Phys.* **2006**, 124.

(33) West, A. M. A.; Elber, R.; Shalloway, D. *J. Chem. Phys.* **2007**, 126.

(34) Elber, R. *Biophys. J.* **2007**, *92*, L85.

(35) Vanden Eijnden, E.; Venturoli, M.; Ciccotti, G.; Elber, R. *J. Chem. Phys.* **2008**, *129*, 174102.

(36) Cardenas, A. E.; Elber, R. *Proteins: Struct., Funct., Genet.* **2003**, *51*, 245.

(37) Akiyama, S.; Takahashi, S.; Kimura, T.; Ishimori, K.; Morishima, I.; Nishikawa, Y.; Fujisawa, T. *Proc. Natl. Acad. Sci. U.S.A.* **2002**, *99*, 1329.

(38) Truhlar, D. G.; Garrett, B. C.; Klippenstein, S. J. *J. Phys. Chem.* **1996**, *100*, 12771.

(39) Olender, R.; Elber, R. *J. Mol. Struct.: THEOCHEM* **1997**, *398*, 63.

(40) Huo, S. H.; Straub, J. E. *J. Chem. Phys.* **1997**, *107*, 5000.

(41) Schlitter, J.; Engels, M.; Kruger, P.; Jacoby, E.; Wollmer, A. *Mol. Simul.* **1993**, *10*, 291.

(42) Cho, S. S.; Levy, Y.; Wolynes, P. G. *Proc. Natl. Acad. Sci. U.S.A.* **2006**, *103*, 586.

(43) Nowak, W.; Czerminski, R.; Elber, R. *J. Am. Chem. Soc.* **1991**, *113*, 5627.

(44) Ulitsky, A.; Elber, R. *J. Chem. Phys.* **1990**, *92*, 1510.

(45) Jonsson, H.; Mills, G.; Jacobsen, K. W. Nudged elastic band method for finding minimum energy paths of transitions. In *Classical and Quantum Dynamics in Condensed Phase Simulations*; Berne, B. J., Ciccotti, G., Coker, D. F., Eds.; World Scientific: Singapore, 1998; p 385.

(46) E, W. N.; Ren, W. Q.; Vanden-Eijnden, E. *Phys. Rev. B* **2002**, *66*, 4.

(47) Elber, R.; Roitberg, A.; Simmerling, C.; Goldstein, R.; Li, H. Y.; Verkhivker, G.; Keasar, C.; Zhang, J.; Ulitsky, A. *Comput. Phys. Commun.* **1995**, *91*, 159.

(48) Vanden-Eijnden, E.; Venturoli, M. Submitted for publication.

(49) Feig, M.; Karanicolas, J.; Brooks C. L. *MMTSB Tool Set*; The Scripps Research Institute: La Jolla, CA, 2001.

(50) Elber, R.; Karplus, M. *Chem. Phys. Lett.* **1987**, *139*, 375.

(51) Czerminski, R.; Elber, R. *Int. J. Quantum Chem.* **1990**, 167.

(52) Onufriev, A.; Bashford, D.; Case, D. A. *Proteins: Struct., Funct., Bioinf.* **2004**, *55*, 383.

(53) Jorgensen, W. L.; Chandrasekhar, J.; Madura, J. D.; Impey, R. W.; Klein, M. L. *J. Chem. Phys.* **1983**, *79*, 926.

(54) Ryckaert, J. P.; Ciccotti, G.; Berendsen, H. J. C. *J. Comput. Phys.* **1977**, *23*, 327.

(55) Weinbach, Y.; Elber, R. *J. Comput. Phys.* **2005**, *209*, 193.

(56) Jorgensen, W. L.; Tiradorives, J. *J. Am. Chem. Soc.* **1988**, *110*, 1657.

(57) Essmann, U.; Perera, L.; Berkowitz, M. L.; Darden, T.; Lee, H.; Pedersen, L. G. *J. Chem. Phys.* **1995**, *103*, 8577.

(58) Abrams, J. B.; Tuckrman, M. E., Martyna, G., J. *Computer Simulations in Condensed Matter: From Materials to Chemical Biology*; Springer: Berlin, 2006; Vol. 1.

(59) Jas, G. S.; Eaton, W. A.; Hofrichter, J. *J. Phys. Chem. B* **2001**, *105*, 261.

(60) Honeycutt, J. D.; Thirumalai, D. *J. Chem. Phys.* **1989**, *90*, 4542.

(61) Dima, R. I.; Thirumalai, D. *J. Phys. Chem. B* **2004**, *108*, 6564.